From Ref 5 we quote

$$\frac{U}{U_0} = \exp \frac{-C_D[(\pi/4)r_0^2]}{W \sin\theta} \frac{\rho_0}{2\alpha} e^{-\alpha H} \quad (6)$$

and

$$t_2 - t_1 = \frac{1}{\alpha U_0 \sin\theta} \int_{H_1}^{H_2} \left(\frac{1}{e^{-\alpha H}}\right) \exp \frac{C_D[(\pi/4)r_0^2]}{W \sin\theta} \frac{\rho_0}{2\alpha} e^{-\alpha H} \, dH \quad (7)$$

Following the procedure outlined in the introduction, the "ballistic length" of the laminar wake of a hemisphere-cylinder of radius r_0 at a given altitude H_2 will be calculated from Eq (2) by making use of the following substitutions: $h(x,0)/RT_0$ will be equal to the value it has at the altitude

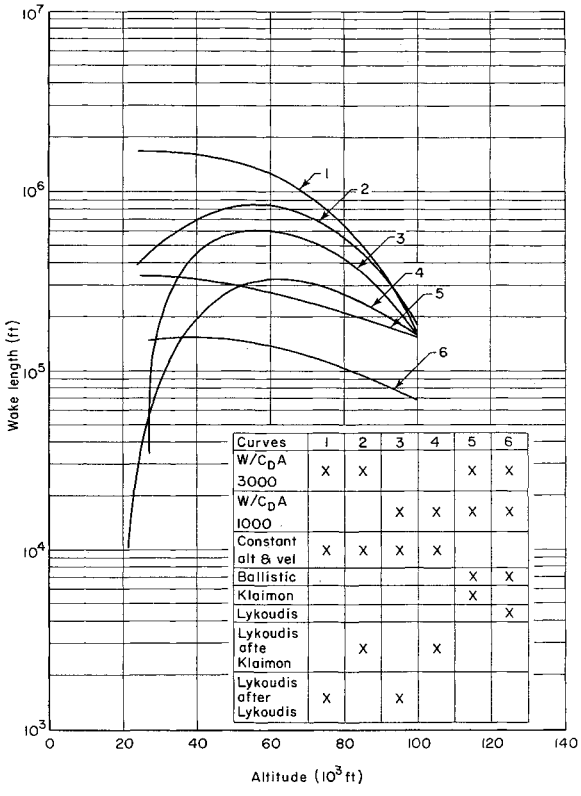

Fig 1 Wake length based on $n_e = 10^7$ electrons/cm^3 and a hemisphere cylinder configuration 30 cm in radius

H_1 so that the electron concentration will be n_e The density ratio ρ_∞/ρ_0 will be evaluated at the same point The quantity $[h(0,0)/RT_0]$ may be evaluated either by using direct gas tables or by making use of the formula provided by Eq (3); the velocity will be the one yielded by Eq (6) for the altitude H_1 The quantity x will be made equal to $U_1(t_2 - t_1)$ and the time interval $(t_2 - t_1)$ will be computed from Eq (7) †

From the foregoing it becomes evident that Eq (2) contains H_1 as the only unknown, however no formal solution is possible; on the other hand a few guesses are sufficient before Eq (2) can be satisfied

After the evaluation of H_1, the "ballistic length" of the trail, based on the electron concentration n_e, is given by the simple relation $L_1 = (H_1 - H_2)/\sin\theta$

† Equations (6) and (7) can be substituted by ballistic data such as those published in Ref 6

3 Examples and Conclusions

Figure 1 shows the numerical results obtained by using the method previously described for the calculation of the "ballistic length" of the wake for the case of two ballistic coefficients, namely, $W/C_DA = 1000$ and 3000 The initial conditions taken for the re-entry are at an angle with the horizontal of 20° and a re-entry velocity of 23,900 fps starting the trajectory at an altitude of 400,000 ft This is the case studied in detail in Ref 6 For both ballistic coefficients it was found that the length remains remarkably the same, as already found in Ref 1 If one compares this result with the "constant altitude and velocity length," then the dependence of the ballistic coefficient is very strong for the latter This behavior can be explained as follows Given an altitude, the trajectory with the smaller ballistic coefficient will have a smaller velocity and hence will have a smaller amount of kinetic energy to dissipate From Eq (2) it can be seen that the "constant altitude and velocity length" will depend directly and solely on this energy On the other hand, the "ballistic length" corresponding to a given altitude depends on the history traced downstream during the re-entry, and hence the ballistic coefficient becomes less significant if the tail of the wake is located at an altitude where the trajectories are not yet strongly dependent on the ballistic coefficient As a matter of fact, in this last case a quick estimate of the "ballistic length" may be obtained by solving Eq (2) for the density ratio ρ_∞/ρ_0 using a rough guess for the time interval $(t_2 - t_1)$ and the initial re-entry velocity

Figure 1 shows also the numerical data of Ref 1 The trend for all the cases studied in common are the same, but the numerical values seem to be apart by a factor of two

References

[1] Klaimon, J H, "The re entry wake in an earth-fixed coordinate system," AIAA Paper 63-185 (June 17–20, 1963)

[2] Lykoudis, P S, "Theory of ionized trails for bodies at hypersonic speeds," The Rand Corp, RM-2682-PR (May 1961)

[3] Feldman, S, "On trails of axisymmetric hypersonic blunt bodies flying through the atmosphere," J Aerospace Sci 28, 6 (1961)

[4] Lykoudis, P S, "The growth of the hypersonic turbulent wake behind blunt and slender bodies," The Rand Corp, RM-3270 PR (January 1963)

[5] Gazley, C, Jr, "Heat transfer aspects of the atmospheric re entry of long range ballistic missiles," The Rand Corp, R-273 (August 1, 1954)

[6] Morris, D N and Benson, P, "Data for ICBM re entry trajectories," The Rand Corp, RM 3475-ARPA (April 1963)

Production of Intense Radiation Heat Pulses

J F Louis,* R Decher,† and T R Brogan‡
Avco-Everett Research Laboratory, Everett, Mass

At the re-entry velocities typical of interplanetary flights, it is likely that very high heat transfer rates to the entering vehicle will be encountered due to radiation from the hot gases surrounding the body [1 2] These rates can approach 50 kw/cm^2 in some cases In order to study the behavior of protective materials for this environment, it is desirable that steady-state simulation of the conditions be provided in the

Received October 10, 1963 This work was partially supported by NASA under Contract No NAS W 697

* Principal Research Engineer
† Engineer Member AIAA
‡ Principal Research Scientist

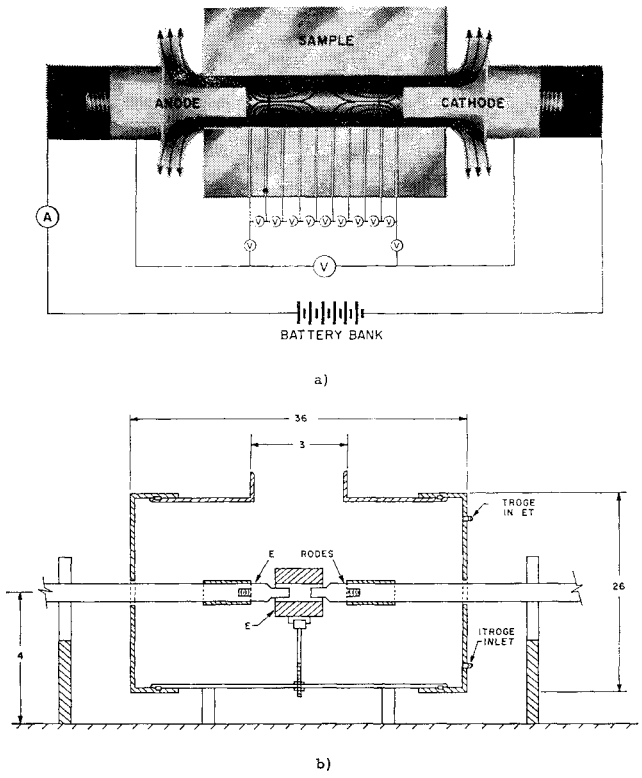

Fig 1 a) Principle of operation of the radiation heat-transfer facility b) Sketch of the second facility

laboratory This work has been directed to this simulation Under the program, a method of producing intense radiation heating has been developed, and materials have been subjected to radiative heat pulses at varying levels up to 51 kw/cm^2 (45,000 Btu/ft^2-sec) and at ambient pressures up to 4 atm absolute Values for heats of ablation (Q^*) have been obtained More work is required to understand fully the results and, in particular, to relate them directly to the flight situation

Figure 1a is a schematic diagram of the facility which has been developed It consists of a high-powered arc surrounded by the material to be tested A cylindrical hole is bored through the test sample and the electrodes are located at its ends as shown When the arc is struck, the discharge column fills most of the volume of the hole The total power into the arc is equal to the product of the current I by the arc voltage V With the enclosed arc configuration, there are three ways the power can be dissipated: 1) electrode losses, 2) absorption by the test material (heating, melting, vaporization), and 3) superheating of material vaporized from the test specimen (and electrodes)

In actual operation, the arc burns in the vaporized material ablated from the test specimen and the graphite electrodes The pressure in the arc column rises above the ambient pressure, and the superheated ablated material is discharged through the passage between the electrode and the test material

The pressure is determined by the rate of material vaporization, the temperature of the arc, and the size of the clearance between the electrodes and the test sample In the center of the test specimen, aerodynamic stagnation conditions prevail as shown, and the joule heat dissipated in the center of the arc column falls onto the boundary, i e , low temperature vaporized material and the wall The streamlines shown in Fig 1a indicate that convection of ablated material plays an important role on the heat actually transferred to the test specimen In this respect, the simulation strongly resembles the flight situation where the combination of radiation from the hot gas through the ablated material to the body, absorption of this radiation in the cooler gas near the body, and the aerodynamic convection, through its influence on the thickness of the ablation layer, will determine the heat-absorbing capacity of the material

During a test, the total current I is measured, as well as the local electric field E, along the wall using the probes shown in Fig 1a Thus, the local power dissipated in the arc column is determined by the product of the current density by the local electric field found from the probe voltages Therefore, the average heat-transfer rate $\dot{q}$, falling onto the test specimen can be determined for the center of the test section where stagnation conditions prevail In the usual manner, the effective heat of ablation Q^* is then equal to the ratio of the apparent heat-transfer rate to the mass rate of ablation per unit area

Two versions of the arc-powered simulator have been built to date A 3 3-Mw battery bank was conveniently available as a power supply for the tests The first facility operated at a total power of up to 3 Mw, and at currents up to 22,000 amp for 3 sec, and has been operated for 1 min at 500-kw input The time limitation is basically due to gross changes in test specimen dimension after times dependent on the nature of the test material and the power input A transite pipe with a viewing window surrounds the arc At the end of the run, nitrogen was injected about the specimen to quench any spontaneous combustion of the graphite electrodes and test material However, this was not completely effective, as the nitrogen entrained some air Therefore, a second version with a sealed test section where the material would remain in a nitrogen atmosphere after shutdown was built Figure 1b is a diagram of the second facility This second facility has basically the same configuration and capability as the first except for its internal atmosphere control

As already stated and shown in Fig 1a, the voltage distribution throughout the sample and the current are measured to determine the power density For electrically insulating test materials, voltage probes are introduced in the sample In the case of electrically conducting materials such as graphite, the test section is made of thin washers coated with a thin layer of arc-sprayed alumina to provide the insulation Voltage taps can be made on the washers and the power density determined Pressure measurements have been carried out using a Kistler gage Figure 2 shows the first facility in operation with the high-temperature ablated material streaming out through the clearance between the electrodes and the test specimen

Preliminary tests were carried out on maple wood, Refrasil reinforced phenolic, bonded graphite cloth, graphite, and Teflon Table 1 summarizes these results, giving the total power, the heat-transfer rate, and the heat of ablation

Heat transfer rates up to 51 kw/cm^2 and heats of ablation up to 40,000 cal/g were recorded After the test, the samples were cut and examined for change in dimensions Figure 3

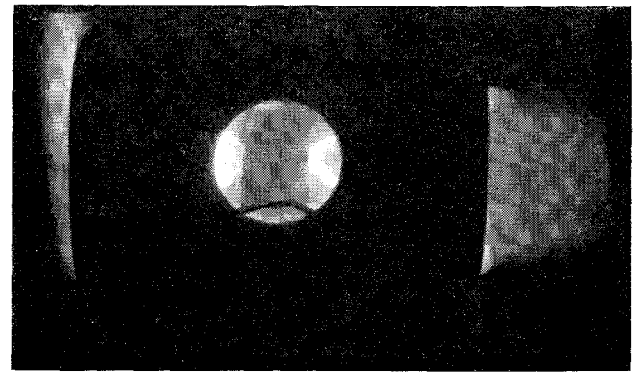

Fig 2 Operation of the radiation heat-transfer apparatus Luminous ablating material is discharging through the clearance between test specimen and electrodes

Table 1 Table of results

Materials	Arc power input, kw	σ, mho/m	$\dot{q}$, kw/cm^2	Q^* cal/g	Q^* Btu/lb
Refrasil reinforced phenolic	2860	3600	51	17300	31400
Refrasil reinforced phenolic	324	3600	2 88	4400	8000
Refrasil reinforced phenolic	965	7160	8 3	6400	11620
Refrasil reinforced phenolic	2250	6480	18	7680	13900
Refrasil reinforced phenolic	3110	6800	22 6	6180	11250
Bonded graphite cloth	2860	3600	51	30000	54500
Maple wood	2320	5100	33	7200	13100
Graphite	2225	3200	20 5	42400	77000
Teflon	2225	3200	20 5	8600	15650

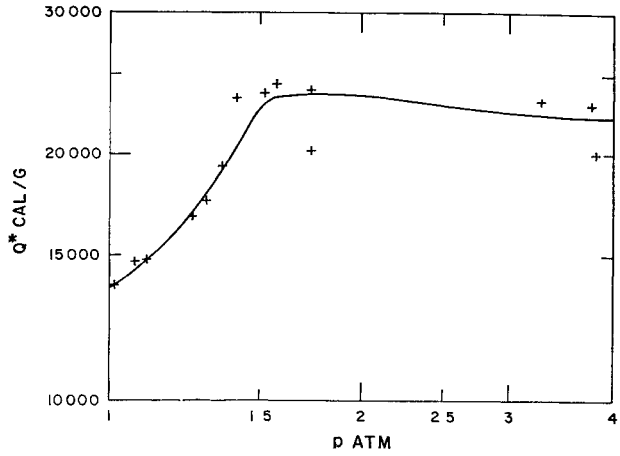

Fig 4 Measured heat of ablation (Q^*) of linen phenolic as a function of pressure

shows the condition of representative samples after test Testing was carried out on linen phenolic at different pressures by changing both the power input and the clearance area The results are plotted on Fig 4 and show that the heat of ablation increases with the pressure up to 1 5 atm At pressures higher than 1 5 atm the heat of ablation Q^* is essentially constant within the scatter of the data Generally speaking, the measured heats of ablation are quite high, indicating an important shielding of the material due to the presence of vaporized absorbent material between the gas and the body, and/or to blowing

To date, diagnosis of the test results has been limited The gas temperature in the arc column has been estimated in several ways with fair agreement By using this estimated temperature, and theoretical studies of gas radiation, it is possible to estimate the radiation heat transfer from the hot arc gas The heat transfer estimated in this manner is in fair agreement with that determined from the electric field-current measurements described previously

Four methods have been used to estimate the temperature in the arc: 1) The effective electrical conductivity of the gas can be calculated from the electric field-current measurements assuming the arc fills the bore of the test specimen Assuming that the ionization is due primarily to carbon vapor with an ionization potential much less than that of the other constituents of the sample, a temperature can be determined from the Saha equation using the measured arc pressure 2) Spectra of the arc column have been taken through windows

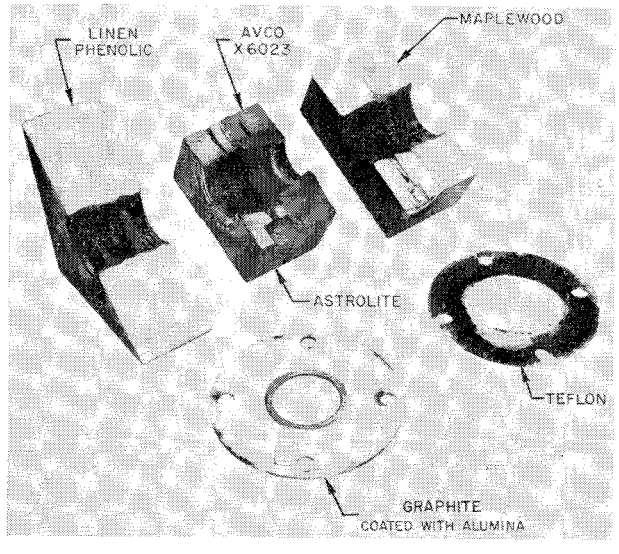

Fig 3 Representative samples following test

in the sample The electron concentration can be determined from the broadening of the hydrogen beta line [3] From this electron density, a temperature can be estimated as described above Since the spectrograph is focused on the center of the arc column, and looks through the thickness of the column, the measured temperature is an effective temperature for radiation 3) Comparison of the intensity of the H_α and H_β lines can be used to estimate an effective radiation temperature 4) From the measurement of the mass rate of ablation and the pressure in the arc column, an average temperature can be calculated since the clearance area between the test sample and the electrodes is known Temperatures determined using the above techniques were in fair agreement ($\pm$ 10%) and varied between 12,000° and 18,000°K depending on the test conditions

The continuum radiation from carbon vapor was determined for a gas temperature of 16,000°K (as determined from apparent gas conductivity) and a pressure of 3 atm [4 5] These conditions correspond to those of the first test listed in Table 1 where the arc power input was 2860 kw and the measured Q^* 17,300 cal/g The continuum radiation calculation, assuming an actual thickness equal to the arc diameter (3 cm), yielded a total radiation heat-transfer rate of 44 kw/cm^2 compared to 51 kw/cm^2 as determined from the electric field-current measurements Thus, the experiment appears relatively self-consistent

The velocity gradient at the stagnation point in the center of the arc column can be estimated from the effective arc temperature, pressure, and the ablation rate The average gas enthalpy can be determined from the temperature estimate and the pressure so that the convective heat transfer in the stagnation region can be estimated [6] Assuming that the specimen wall is at the boiling point of graphite ($\approx$ 4000°K) and for the same conditions for which the radiative transfer was compared with the electric field-current rate, a convective heat transfer of 2 6 kw/cm^2 is indicated Thus, it appears that radiation is the primary heat-transfer mechanism in the apparatus Further, these results, together with the high Q^* values such as those shown in Fig 4, would indicate that body shielding due to absorption by ablated material of substantial optical thickness near the body can be very important

References

[1] Kivel, B and Bailey, K, "Tables of radiation from high temperature air," Avco Everett Res Lab Res Rept 21 (December 1957)

[2] Allen, R A, Rose, P H, and Camac, J C, "Non-equilibrium and equilibrium radiation at super-satellite re entry velocities," Avco-Everett Res Lab Res Rept 165 (September 1962)

[3] Griem, H R, Kolb, A C, and Shen, K Y, "Stark broaden-

ing of hydrogen lines in plasma," National Research Lab Rept 5455 (March 1962)

[4] Unsöld, A , ' Continuous spectrum of high-pressure Hg lamp and similar gas discharges," Ann Physik 33, 607–616 (1938)

[5] Biberman, L M and Norman, G E , "On the calculation of photoionization absorption," Opt i Spektroskopiy 8, 433 (1960); also Opt Spectr (USSR) (English Transl) 8, 230 (1960)

[6] Fay, J A and Kemp, N H , "Theory of stagnation point heat transfer in a partially ionized diatomic gas," Avco-Everett Res Lab Res Rept 144 (April 1963)

A Flow-Separation Spike for Hypersonic Control of a Hemisphere-Cylinder

WILLIAM E THURMAN*
Aerospace Research Laboratories, Wright Patterson Air Force Base, Ohio

Nomenclature

L/D = lift/drag
Re = Reynolds number based on the body diameter and the free stream conditions ahead of the body
s/d = longitudinal arc length measured from the centerline of the body/the diameter of the body
β = reattachment angle measured from the longitudinal centerline of the body, deg
θ = spike deflection angle measured from the centerline of the body, deg
ϕ = angle of each longitudinal ray measured from the direction of the spike deflection clockwise from the front, deg

Introduction

THERE has been considerable interest in the study of hypersonic flows in which a separated region is induced ahead of the body by a flow-separation spike Bogdonoff and Vas[3] were among the first investigators to determine that the spike reduces the form drag and, if the flow remains laminar, lowers the over-all heat transfer to the forebody These results suggest that the spike may have flight applications

The present study investigates the possibilities of using a deflected flow-separation spike to control a body at hypersonic speeds It is a preliminary investigation in that one body shape is tested at only one Mach number and Reynolds number The study determines the lift and drag coefficients that result from the changing spike deflections These coefficients were obtained by integrations of the surface pressures

Experimental Facilities and Model

The experimental investigation was concluded in the Aerospace Research Laboratories' 3-in hypersonic wind tunnel A conical, nominal Mach 12 nozzle that had a Mach number gradient of 0 42/in along the centerline of the open-jet test section was used for the study

The stainless-steel model is schematically shown in Fig 1 It consisted of a right circular-cylindrical afterbody $\frac{1}{2}$ in in diameter, with a hemispherical nose A flow-separation spike, $\frac{1}{16}$ in in diameter, with a spike length to body diameter ratio of 4, extended ahead of the nose of the body This spike length was determined by the authors of Ref 3 to be the optimum spike length for decreasing both the form drag and the over-all heat transfer to the model The model was

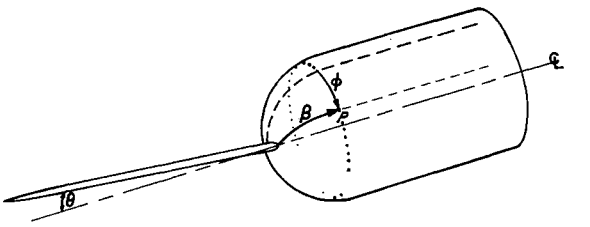

Fig 1 The test model showing angular measurements

equipped with 10 pressure orifices located at various spiral positions about its surface

A double-pass Schlieren system and glow discharge flow-visualization techniques were used for visual studies of the flow field

Test Program

In these studies the centerline of the model was aligned with the centerline of the wind tunnel Only the spike was deflected through an angle that was measured from the centerline of the model The test program was designed to measure in detail the pressure distribution over the model which resulted from the spike deflection Accurate measurement of this pressure distribution required a large number of pressure readings on the body surface, but the maximum number of orifices that could be placed in the model was limited to 10 Therefore, the model was designed with fixed deflection spikes that could be rotated through 360° about the longitudinal axis of the model The model was fixed and the spike rotated

Pressures were recorded as the spike was rotated through 360° in increments of 20° This afforded 180 pressure readings to use for the pressure integration Pressure distributions were measured with 0 spike deflection and with spike-deflection angles measured from the centerline of the model of 47° 5′, 2° 30′, 4° 58′, and 7° 15′

The Reynolds number of the test remained constant at 28,700/in [2] A test Mach number of 11 76 was used with stagnation conditions of 400 psia and 1300°F Although these stagnation conditions might result in air condensation in the test section, a report by Daum[5] indicated that liquefaction did not occur

The longitudinal Mach number gradient along the tunnel centerline was not considered important to the results of this study since 8 of the 10 pressure orifices were within 0 25 in of the spike base Therefore, a Mach number of 11 76 was used for this study This Mach number corresponded to the location of the spike base The choice of a constant Mach number for data reduction did not introduce appreciable errors in the computations of the force coefficients

Pressure Measurements

Examples of some of the curves of pressure distribution that were measured in these tests are given in Fig 2 which shows the curves of the pressure distribution for each spike-deflection angle along the longitudinal ray opposite to the direction of the spike deflection Also plotted in this figure is the pressure distribution along a longitudinal ray for the straight spike and the modified Newtonian pressure distribution over the hemispherical nose of the body

The shape of the pressure distribution curve for the straight spike is similar to the curve shapes obtained by the authors of Ref 3 at Mach 14 in helium The individual pressure values measured along the model during the present tests are higher than the pressures measured by Bogdonoff and Vas, but these sets of data cannot be accurately compared because the tests were made in a different testing medium and at a different Reynolds number

The pressure distribution curves that were obtained by Crawford[4] are similar to the straight spike pressure distribution curves that were measured in these tests A comparison

Received October 2, 1963

* Captain, U S Air Force, and Research Aerospace Engineer, Hypersonic Research Laboratory